Biosensors and Bioelectronics 74 (2015) 953–959

Contents lists available at ScienceDirect

Biosensors and Bioelectronics

journal homepage: www.elsevier.com/locate/bios

Ultrasensitive electrochemical biosensor based on reduced graphene oxide-tetraethylene pentamine-BMIMPF$_6$ hybrids for the detection of α2,6-sialylated glycans in human serum

Yuliang Li [1], Junlin He [1], Yazhen Niu, Chao Yu *

Institute of Life Science and School of Public Health, Chongqing Medical University, Chongqing 400016, PR China

ARTICLE INFO

Article history:
Received 14 June 2015
Received in revised form
26 July 2015
Accepted 30 July 2015
Available online 31 July 2015

Keywords:
α2,6-sialylated glycans
Sambucus nigra agglutinin
Bimetallic AuPt alloy nanoparticles
BMIMPF$_6$

ABSTRACT

In this paper, a simple, ultrasensitive and label-free electrochemical α2,6-sialylated glycans biosensor based on reduced graphene oxide-tetraethylene pentamine-1-butyl-3-methylimidazolium hexafluorophosphate (BMIMPF$_6$) hybrids was developed. Due to the abundance of amino groups from reduced graphene oxide-tetraethylene pentamine (rGO-TEPA) and the electrostatic interaction of BMIMPF$_6$, bimetallic gold platinum alloy nanoparticles (AuPtNPs) were densely adsorbed onto the surface of the nanocomposite, providing a large surface area available for the immobilization of *Sambucus nigra agglutinin* (SNA). AuPtNPs have excellent conductivity and catalytic activity, which can promote electron transfer between the electrolyte solution and the surface of electrode and can enhance the sensitivity of biosensor. SNA, which specifically binds α2,6-sialylated glycans, was covalently immobilized on AuPtNPs for specific detection of α2,6-sialylated glycans in human serum. Under optimal experimental conditions, amperometric response changes were used to detect α2,6-sialylated glycans with a broad linear range of 10 fg mL^{-1}–1 μg mL^{-1} and a low detection limit of 3 fg mL^{-1} ($S/N=3$). When applied to spiked serum samples, the recovery of the developed biosensor ranged from 100.8% to 101.4%, suggesting that the electrochemical biosensor would be suitable for the practical detection of α2,6-sialylated glycans.

1. Introduction

Sialic acid (Sia), or N-acetylneuraminic acid (Neu5Ac), is a common moiety at terminal monosaccharides attached to cell surface glycoconjugates (Kim et al., 2011). The α2,6-linkage of sialic acid to N-acetyllactosamine structures (Galβ1-4GlcNAc) is a Golgi-mediated process mediated by β-galactoside α2,6-sialyltransferase (ST6Gal-I) (Harduin-Lepers et al., 2001; Kim et al., 2011). Variants of α2,6-sialylation, the outermost monosaccharides on the glycan chains of glycoproteins and glycolipids, are associated with wide biological and pathological disorders, including the development and progression of some cancers (Dall'Olio et al., 1989; Petretti et al., 1999). When carcinoma cells undergo apoptosis, α2,6-sialylated glycans are formed and released into the blood resulting in increased concentration in human serum. In addition, high levels of α2,6-sialylation have been detected in certain tumors (Gessner et al., 1993). Therefore, α2,6-sialylated glycans are important molecular targets for cancer diagnosis and are an extensively studied clinical cancer biomarker (Dall'Olio et al., 1989).

The remarkable chemical diversity of sialylated glycans (α2,3, α2,6, α2,8) has resulted in multiple enzymatic mechanisms (Boltje et al., 2009; Kim et al., 2011). Therefore, glycans are difficult to detect and quantify in serum. Recombinant soluble forms of α2,6-sialylated glycans (Neu5Acα(2-6)Gal β MP glycoside), α2,6-linkages of sialic acids to N-acetyllactosamine structures in glycoconjugates, can be recognized by specific lectins. Certain Sia-binding lectins have been demonstrated to be powerful tools for detecting Sia-specific glycoconjugates as a result of ligand promiscuity. For example, *Limax flavus agglutinin* and *Wheat germ agglutinin* have been used to detect sialylated glycoconjugates (Gao et al., 2014). *Sambucus nigra agglutinins* (SNAs) are an ideal tool for detecting α2,6-sialylated glycans (Park et al., 2012; Shibuya et al., 1987). Conventional analytical methods used for detecting sialylated glycans primarily include high-performance liquid chromatography-mass spectrometry (Harvey, 2011; Lamari et al., 2003), gas chromatography-mass spectrometry (Bratosin et al., 2007; Zanetta et al., 2011; Kim et al., 2006), nuclear

* Correspondence to: Box 174#, Institute of Life Sciences, Chongqing Medical University, No.1 Yixueyuan Road, Yuzhong District, Chongqing 400016, PR China; Fax: 86 23 68486294.
E-mail address: yuchaom@163.com (C. Yu).
[1] Contributed equally to this work.

http://dx.doi.org/10.1016/j.bios.2015.07.073
0956-5663/

magnetic resonance spectroscopy (Jones, 2005), and capillary electrophoresis (Lamari et al., 2003; Liu et al., 2001). However, no methods exist for the specific detection of α2,6-sialylated glycans. In this regard, a novel method capable of rapid, simple, sensitive and differentiated detection of α2,6-sialylated glycans is required.

To increase the sensitivity of electrochemical biosensors for biomarker detection, considerable efforts have been devoted to immobilizing bio-components and amplify signals (Yuan et al., 2015). Reduced graphene oxide-tetraethylene pentamine (rGO-TEPA) is a new material that consists of rGO covalently bonded to tetraethylene pentamine (Wu et al., 2015; Zhang et al., 2014). This combination retains the original properties of rGO while improving water solubility and stability (Guo et al., 2015; Wu et al., 2014). In addition, rGO-TEPA contains many amino groups, making it an ideal template for loading metal nanoparticles or metal ions to enhance its performance further. The structure of rGO-TEPA is shown in Fig. S1. Room temperature ionic liquids (RTILs), are green solvents that are gaining increasing attention in electroanalytical chemistry as a result of their negligible vapor pressure, outstanding chemical, thermal stability, high conductivity, and low toxicity (Buzzeo et al., 2004; Shafiquzzaman Siddiqueea et al., 2014). $BMIMPF_6$ is a hydrophobic RTIL that may form a hydrophobic membrane when coated on an electrode surface to avoid the direct contact with a buffer solution (Zheng et al., 2007). In this manner, the rGO-TEPA immobilized on the electrode cannot leach from the electrode surface. $BMIMPF_6$ can further prevent aggregation of rGO-TEPA due to cation–π interactions of $BMIMPF_6$ with rGO-TEPA. The structure of $BMIMPF_6$ is shown in Fig. S2. Recently, bimetallic alloys have also attracted considerable attention for the fabrication of electrochemical sensors. Bimetallic alloys can aid in retaining the functional properties of each component and may offer synergistic effects via cooperative interactions, resulting in desired features including increased surface area, enhanced electrocatalytic activity, and higher invulnerability to intermediate species (Safavi and Farjami, 2011; Zhang et al., 2014). Cao and co-workers have reported an application of a novel immunosensor based on bimetallic AuPt nanochains (AuPtNCs), anti-carcinoembryonic antigens, and horseradish peroxidase as a label for the detection of carcinoembryonic antigens (Cao et al., 2013). The electrochemical signal was significantly amplified using AuPtNCs. Bimetallic gold platinum alloy nanoparticles, also provide higher catalytic activity toward H_2O_2 (Jia et al., 2014). Considering this feature, we pursued a green method to synthesize gold platinum alloys by electrodeposition and their subsequent use in an electrochemical biosensor.

Electro-deposition is the most controllable and robust technique for the synthesis of metal nanoparticles (NPs), in which the density, size, alloy composition and even shape of NPs can be strictly controlled by electro-deposition time, potential, concentration, and composition of metal precursor solutions (Claussen et al., 2009; Yang et al., 2010). With the aim of exploring the excellent film-forming ability and the good conductivity of $BMIMPF_6$ and the affinity of AuPtNPs toward SNA, we used a rGO-TEPA-$BMIMPF_6$ nanocomposite film as an immobilization matrix to fabricate an electrochemical biosensor with the finding that the biosensor exhibited excellent electrochemical response to detect α2,6-sialylated glycans.

2. Experimental

2.1. Materials and reagents

Reduced graphene oxide-tetraethylene pentamine (rGO-TEPA) was purchased from Nanjing XIANFENG Material TECH Co., Ltd. Neu5Acα(2-6)Gal β MP glycoside and Neu5Acα(2-3)Gal β MP glycoside was purchased from Tokyo Chemical Industry. *Sambucus nigra agglutinin* was purchased from Gentaur (Kampenhout, Belgium, www.gentaur.com). $HAuCl_4 \cdot 3H_2O$, $H_2PtCl_4 \cdot 6H_2O$, 1-butyl-3-methylimidazolium hexafluorophosphate ($BMIMPF_6$), bovine serum albumin (BSA, 96–99%) and β-cyclodextrin (β-CD) were obtained from Sigma-Aldrich (St. Louis, USA, www.sigmaaldrich.com). Dopamine (DA), L-cysteine, uric acid (UA) and ascorbic acid (AA) and glucose were purchased from Aladdin (Shanghai, China, www.aladdin-e.com). Doubly distilled water was obtained from a Millipore Mill-Q purification system. Other chemicals were analytical grade and used without further purification.

2.2. Apparatus and measurements

The electrochemical experiments were performed an electrochemical workstation (CHI660E) with a three-electrode system (Shanghai Chenhua Apparatus Corporation, China). A glassy carbon electrode (GCE, 4 mm in diameter) was used as the working electrode, with platinum serving as the counter electrode, and a saturated calomel electrode (SCE) serving as the reference electrode. Electrochemical impedance spectroscopy (EIS) was performed in 5 mmol L^{-1} $[Fe(CN_6)]^{3-/4-}$ solution in the frequency range of 0.01–10^5 Hz. Scanning electron microscopy (SEM) was performed using Hitachi-7500518 (Hitachi Limited, Japan). Energy dispersive X-ray spectroscopy (EDS) was measured using a JEOL JSM-6700F microscope (Japan). Fourier transform-infrared (FT-IR) spectrum was obtained from a NICOLET-20sx spectrometer (Thermo Nicolet, USA).

2.3. Preparation of rGO-TEPA-$BMIMPF_6$ nanocomposite

First, rGO-TEPA (1 mg mL^{-1}) was dissolved in a β-CD (2 mg mL^{-1}) solution by sonicating for 2 h. Then, varying amounts of ionic liquid ($BMIMPF_6$) were added to the mixture using magnetic stirring until a dark homogeneous solution was obtained.

2.4. Fabrication of the biosensor

Prior to modification, the glassy carbon electrode (GCE) was polished with 0.3 and 0.05 μm alumina powder sequentially until a mirror-like surface was obtained and was consecutively sonicated with absolute ethanol and ultrapure water for 5 min. The fabrication of the electrochemical biosensor is outlined in Scheme 1. Initially, 6 μL of the rGO-TEPA-$BMIMPF_6$ nanocomposite was added to the surface of the GCE. After the electrode dried at room temperature, it was immersed in a $HAuCl_4/H_2PtCl_6$ (10 mM, 3:1) solution with −0.25 V for 400 s to electrodeposit gold platinum alloy nanoparticles (DpAuPtNPs) on the electrode (Fei et al., 2009). SNA (6 μL, 2.0 mg mL^{-1}) was added to the platform and incubated for overnight at 4 °C. Finally, a solution of 1% BSA was coated onto the modified electrode for 1 h to block nonspecific binding sites. After each step, the modified electrode was cleaned with ultrapure water thoroughly. All fabricated electrodes were stored at 4 °C when not in use.

2.5. Electrochemical measurements

Six microliters of varying concentrations of Neu5Acα(2-6)Gal β MP glycoside standard solutions or dilution samples were added to the fabricated biosensor and incubated for 150 min at room temperature. The residual compounds were removed with doubly distilled water. Electrochemical responses of the modified electrode were recorded using amperometric measurements at E = −0.4 V in PBS (pH 7.4). After the background current was stabilized under gentle stirring, 1 mol L^{-1} H_2O_2 in PBS was added and the difference in current was recorded.

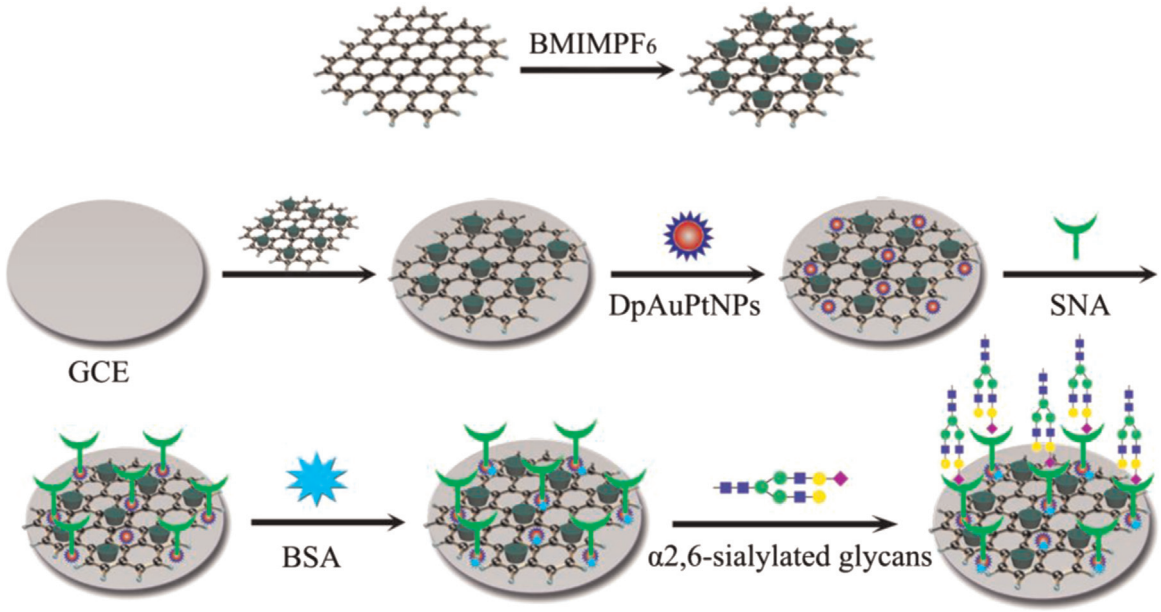

Scheme 1. Schematic representation of the electrochemical biosensor.

3. Results and discussion

3.1. Characterization of prepared material and DpAuPtNPs

As shown in Fig. 1A and B, rGO-TEPA had a wrinkled, paper-like structure and morphology. RGO-TEPA had a large surface area that was favorable for electron transfer. Furthermore, rGO-TEPA contains amino groups which aided in the immobilization of a large number of metal nanoparticles, thereby increasing the sensitivity of the electrode. The FT-IR spectrum of rGO-TEPA (Fig. S3) contained a strong and broad absorption peak at 3425 cm^{-1}, which was ascribed to the stretching vibration of N–H. Bimetallic AuPt alloy nanoparticles deposited on the surface of the rGO-TEPA modified electrode with the assistance of both the amino groups of rGO-TEPA and the electrostatic interaction of $BMIMPF_6$. These nanoparticles were monodispersed and had globular morphology, forming an interpenetrating network with favorable conduction pathways for electron transport (Fig. 1C and D). Interestingly, DpAuPtNPs were more prone to deposit in large quantities at rGO-TEPA sheets, which were wrinkled or curled into tubular structures. This may be attributed to higher static attractions during synthesis, a mechanism which is similar to that reported for electrochemically reduced graphene oxide (ERGO) (Yang et al., 2011) and multi-walled carbon nanotubes (MWCNTs) (Yang et al., 2010).

3.2. Electrochemical characterization of AuPtNPs

Fig. 1E shows the cyclic voltammograms (CV) of the bare GCE, rGO-TEPA-$BMIMPF_6$ modified electrode, and AuPtNPs/rGO-TEPA-$BMIMPF_6$ modified electrode in a 0.5 M H_2SO_4 solution. The peaks are associated with the reduction of oxide species on the electrode surface, and can be used to determine the surface composition. The reduction peak began at 0.3 V, corresponding to Pt species, and the second peak at 0.8 V was associated with Au species (Browna et al., 2008; Zan et al., 2013). Using the Randles–Sevcik equation (Xie et al., 2015; Zan et al., 2013), the surface area of the DpAuPtNPs/rGO-TEPA-$BMIMPF_6$ modified electrode was calculated to be 56.87 mm^2, which is 4.5 times that of the bare GCE. Elemental compositions of AuPtNPs/rGO-TEPA-$BMIMPF_6$ were analyzed by EDS (Fig. 1F). Signature peaks for C, N, Au and Pt were observed for AuPtNPs/rGO-TEPA-$BMIMPF_6$, indicating that Au and Pt can both be successfully produced electrochemically under the conditions utilized and contribute equally to the formation of bimetallic NPs during the synthesis. To demonstrate the significance of DpAuPtNPs in the fabricated biosensor for signal amplification, the GCE was coated with various metal nanoparticles including AuNPs, PtNPs and AuPtNPs (Fig. S4.). It was observed that depositing AuPtNPs as the catalysis medium provided a much greater response in comparison with other media, which may be a result of the following causes: first, rGO-TEPA with a high surface area may increase the potential load of AuNPs and PtNPs; second, PtNPs have higher catalytic activity toward H_2O_2 reduction; and third, $BMIMPF_6$, AuNPs and PtNPs have high electrical conductivity which can more efficiently facilitate electron transfer.

3.3. Electrochemical characterization of the stepwise-modified electrode

Electrochemical impedance spectroscopy (EIS) was employed to monitor the stepwise fabrication processes of the immunosensor using $[Fe(CN)_6]^{3-/4-}$ as a redox probe. EIS was used to investigate the interface properties of a modification of the electrode. The impedance spectra include a linear portion and a semicircle portion. The linear portion at lower frequencies corresponds to the diffusion-limited process, and the semicircle portion at higher frequencies represents the electron transfer limited process. The semicircle diameter equals the electron-transfer resistance (R_{et}). Fig. 2A shows that the bare GCE exhibited a small semicircle at high frequency (curve a) of R_{et} value (196.1 Ω). After the electrode was modified with rGO-TEPA-$BMIMPF_6$, the resistance was much less than that of the bare GCE (curve b, R_{et}=77.99 Ω). This implied that the rGO-TEPA-$BMIMPF_6$ formed an interpenetrating network in favor of interfacial and redox probe electron transfer (Stobiecka and Hepel, 2011). The resistance continued to decrease as rGO-TEPA-$BMIMPF_6$ was further modified with AuPtNPs (curve c, R_{et}=39.71 Ω). This demonstrated that AuPtNPs were excellent electron transfer interfaces between the electrolyte solution and the electrode surface. After incubation with SNA, the R_{et} was significantly enlarged (curve d, R_{et}=573.1 Ω), which indicates that

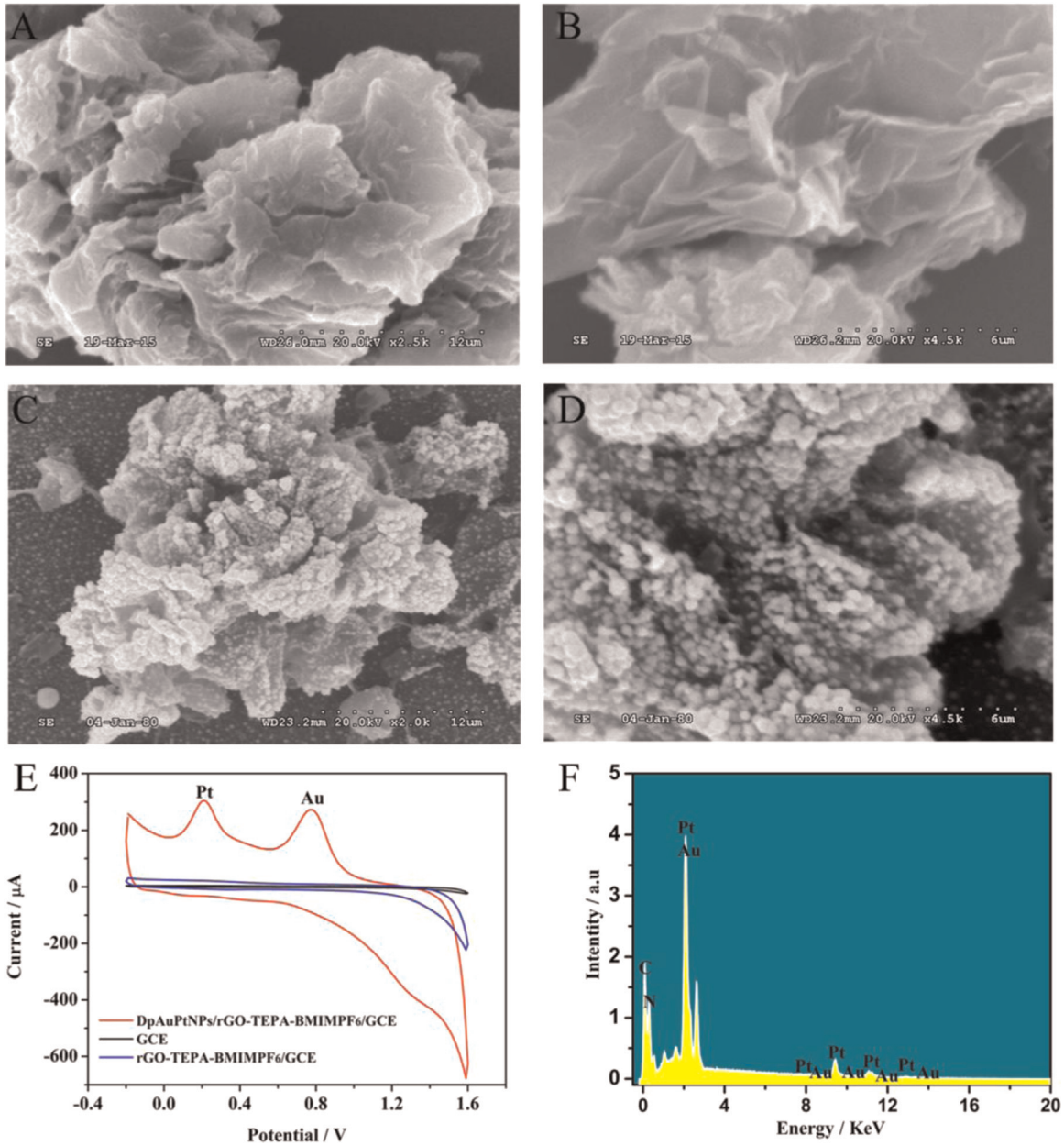

Fig. 1. SEM image of rGO-TEPA (A and B) and AuPtNPs (C and D); (E) Cyclic voltammograms of the bare GCE, rGO-TEPA-BMIMPF$_6$ modified electrode and DpAuPtNPs/rGO-TEPA-BMIMPF$_6$ modified electrode in deaerated 0.5 M H_2SO_4. Scan rate: 50 mV s^{-1}. (F) EDS spectra of AuPtNPs/rGO-TEPA-BMIMPF$_6$.

SNA was immobilized on the modified electrode successfully and blocked electron transfer. A larger semicircle diameter of curve e was later found (R_{et}=1439 Ω), confirming that the prepared biosensor was blocked with BSA. Subsequently, the R_{et} of curve f increased again (R_{et}=1905 Ω), indicating the successful capture of Neu5Acα(2-6)Gal β MP glycoside and the formation of a complex layer blocking electron transfer. The inset in Fig. 2A (top right corner) is the equivalent circuit applied to fit the impedance spectra. This circuit includes the resistance of the electrolyte solution, R_s, the electron transfer resistance, R_{et}, the constant phase element CPE related to the double layer capacitance, C_{dl}, and the Warburg impedance, Z_w, which is a cause of the diffusion of the redox probe ions to the electrode interface from the bulk of the electrolyte. The values obtained after fitting resistance spectra are recorded in Table 1. Simultaneously, cyclic voltammetry was employed to monitor the stepwise fabrication process of the biosensor. As shown in Fig. 2B, the data are in agreement with the result obtained from EIS, indicating the successful fabrication of the biosensor.

The influence of the potential scan rate on the peak current response at DpAuPtNPs/rGO-TEPA-BMIMPF$_6$ electrode was also investigated. Fig. S5(A) shows that the redox peak current increased gradually as the scan rate increased from 20 to 120 mV s^{-1}. In addition, both cathodic and anodic peak currents were proportional to the square root of the scan rates in Fig. S5(B). According to the Randles–Sevcik equation, this result indicates that the redox reaction on the electrode surface was a diffusion-controlled process, which is consistent with previously reported results (Muller and Lambert, 2011; Zhang et al., 2015).

3.4. Optimization of experimental conditions

The electrochemical performance of the Neu5Acα(2-6)Gal β MP glycoside biosensor may be influenced by many factors, such as the concentration of BMIMPF$_6$, the volume of nanocomposite, the length of time for AuPtNPs electro-deposition, the length of

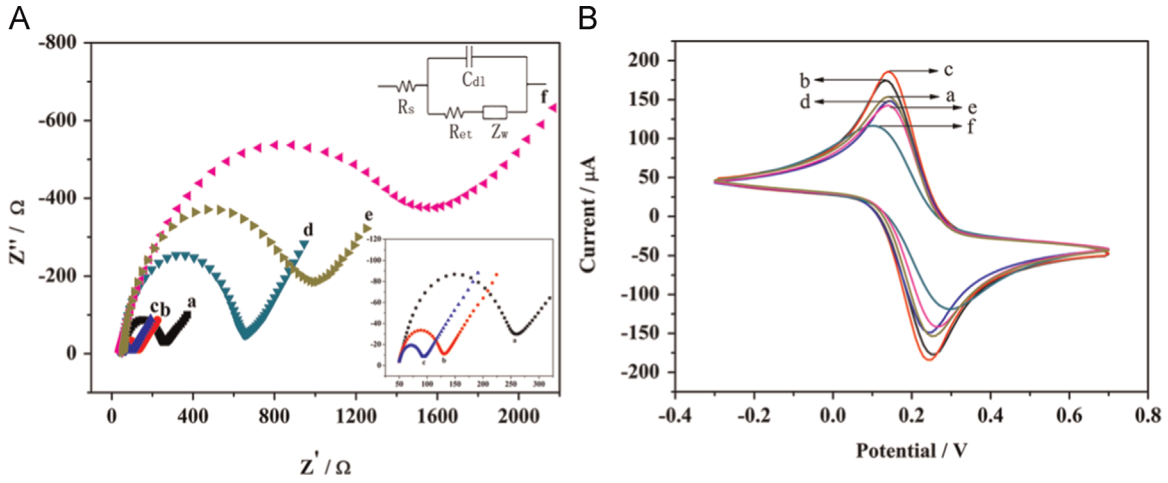

Fig. 2. Typical EIS (A) and CV (B) studies of $[Fe(CN)_6]^{3-/4-}$ (5 mM, 1:1) in 10 mM PBS (pH 7.4) for (a) a bare electrode, (b) rGO-TEPA-$BMIMPF_6$/GCE, (c) DpAuPtNPs/rGO-TEPA-$BMIMPF_6$/GCE, (d) SNA/DpAuPtNPs/rGO-TEPA- $BMIMPF_6$/GCE, (e) blocking with 1% BSA and (f) specific recognition with 1 ng ml^{-1} Neu5Acα(2-6)Gal β MP glycoside.

Table 1
Simulation parameters of the equivalent circuit components.

Electrode	R_s (Ω cm^2)	R_{et} (Ω cm^2)	C_{dl} (μF cm^2)	n	$10^3 Z_w$ (Ω cm^2)
GCE	7.17	24.63	31.69	0.89	1.03
rGO-TEPA-$BMIMPF_6$/GCE	6.59	9.80	13.94	0.92	1.01
DpAuPtNPs/rGO-TEPA-$BMIMPF_6$/GCE	6.67	4.99	14.68	0.94	0.31
SNA/DpAuPtNPs/rGO-TEPA-$BMIMPF_6$/GCE	6.23	71.98	15.40	0.92	0.80
blocking with 1% BSA	6.83	180.74	68.74	0.87	0.35
1 ng ml^{-1} Neu5Acα(2-6)Gal β MP glycoside	6.36	239.27	65.16	0.87	0.34

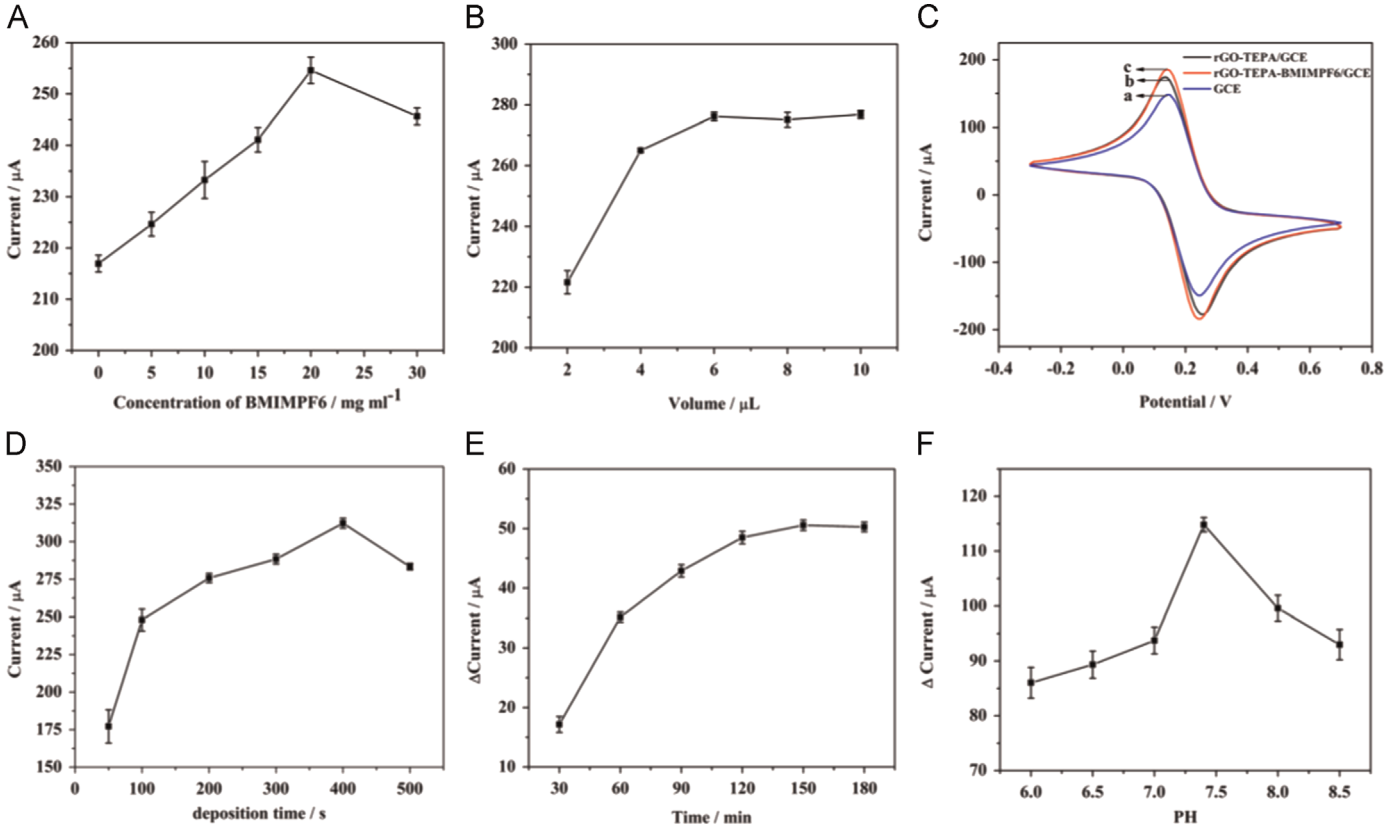

Fig. 3. Effects of (A) concentration of $BMIMPF_6$, (B) volume of nanocomposite, (D) time of AuPtNPs electro-deposition, (E) recognition time on the DPV response and (F) pH of the buffer on amperometric response. Mean values and standard deviations were obtained from at least three experiments. (C) CV of the bare GCE, rGO-TEPA- $BMIMPF_6$/GCE and DpAuPtNPs/rGO-TEPA-$BMIMPF_6$/GCE.

recognition time, and the buffer pH.

The concentration of $BMIMPF_6$ is a rather important factor for biosensor fabrication and could influence its stability and sensitivity. Fig. 3A demonstrates that as the concentration of $BMIMPF_6$ increased from 0 to 20 mg mL^{-1}, the peak current increased, and subsequently decreased after 20 mg mL^{-1}. This effect is due to the high concentration of $BMIMPF_6$ in buffer, which likely created an inhomogeneous mixture.

The volume of nanocomposite was investigated to further improve the sensitivity of the rGO-TEPA-$BMIMPF_6$ biosensor and to provide a favorable platform for electro-deposition of AuPtNPs. The volume of nanocomposite was tested in the range of 2–10 μL. The results in Fig. 3B indicate that the changes in current increased until a volume of 6 μL, then remained stable. Fig. 3C shows the excellent electron-transfer ability of rGO-TEPA-$BMIMPF_6$ in comparison to controls. Therefore, the optimal formation volume of nanocomposite was determined to be 6 μL.

The AuPtNPs electro-deposition time is a critical factor for the layer thickness and quantity of AuPtNPs deposited. This time also plays a key role in providing a favorable surface for SNA immobilization and for catalyzing the H_2O_2 reaction. As shown in Fig. 3D, the current increased from 50 to 400 s, then gradually decreased after 400 s. This is due to the tendency of DpAuPtNPs to aggregate to larger particles or bulk clusters and eliminates the advantage of a larger reactive surface area (Yang et al., 2011). The results of amperometric measurements are in agreement with this conclusion (data not shown). Therefore, 400 s was selected as the optimal deposition time for the experiment.

For recognition of Neu5Acα(2-6)Gal β MP glycoside, incubation time is a notably important parameter. A period of time is required for the SNA to bind the glycoside and form a complex. To study the effect of the incubation time on response signal, the fabricated biosensors were incubated for 30–80 min at room temperature. The results in Fig. 3E indicate that more glycosides were captured by SNA as the length of time increased. When the incubation time was greater than 150 min, the changes in current remained stable, suggesting that the amount of glycoside captured on the surface of the sensor reaches a maximum based on the specific lectin and glycoside reaction. Therefore, 150 min was selected as the optimal incubation time.

The pH of the working buffer is also an important factor affecting biosensor efficiency. To achieve an optimal electrochemical signal, the fabricated biosensor was incubated with 1 ng ml^{-1} Neu5Acα(2-6)Gal β MP glycoside for 150 min, then the biosensor was investigated in a 0.1 M PBS buffer with pH varying from 6.0 to 8.5. As shown in Fig. 3F, the current response increases from 6.0 to 7.4, and decreases from 7.4 to 8.5. This is likely because an alkaline or acidic environment may influence the reaction of H_2O_2. Thus, buffer with a pH of 7.4 was used as the optimized condition for all electrochemical measurements.

3.5. Analysis and detection

Amperometric measurements were used to evaluate the performance of the prepared biosensor incubated with 6 μL of varying concentrations of Neu5Acα(2-6)Gal β MP glycoside under optimized conditions. Increasing concentrations of Neu5Acα(2-6)Gal β MP glycoside caused, increasing amounts of the lectin-glycoside complexes to be formed, which gradually hindered the catalytic reaction. Therefore, the catalytic response decreased. The change in the catalytic response is directly related to the amount of glycoside captured on the electrode surface. As shown in Fig. 4, the equation of the calibration plot was separated into two parts. Below values of 1 ng mL^{-1}, the equation used was ΔCurrent (μA) = −7.88 + 20.77 log C, R^2 = 0.994. Over 1 ng mL^{-1}, the equation used was ΔCurrent (μA) = −104.07 + 36.54 log C, R^2 = 0.999. The

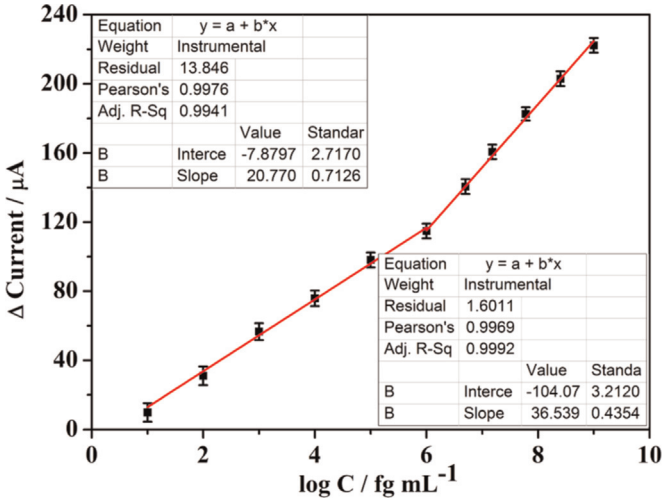

Fig. 4. Calibration curve of the biosensor toward different concentration of Neu5Acα(2-6)Gal β MP glycoside.

detection limit was estimated to be 3 fg mL^{-1} (S/N = 3). The detection limit and linear range of the fabricated biosensor were compared with previously reported methods in Table S1 and S2, and illustrate that the fabricated biosensor has a lower detection limit.

3.6. Selectivity, stability and reproducibility of the electrochemical biosensor

To evaluate the selectivity of the proposed biosensor, endogenous molecules such as glucose, ascorbic acid, uric acid, L-cysteine, dopamine and Neu5Acα(2-3)Gal β MP glycoside were used to confirm that the change in current was a result of the specific recognition of Neu5Acα(2-6)Gal β MP glycoside and its lectin. The change in current caused by interfering substances was less than 6% of that without these compounds (Fig. S6), indicating that the selectivity of the biosensor was acceptable.

The DpAuPtNPs/rGO-TEPA-$BMIMPF_6$ modified biosensor was stored in a refrigerator at 4 °C. After storage for 7 and 14 days, the change in current retained 93.35% and 91.47% of its original current change, respectively. This stability may be due to biocompatibility of bimetallic AuPt alloy nanoparticles.

Reproducibility of the electrochemical biosensor was also evaluated. The intra-assay precision of the biosensor was estimated by analyzing three Neu5Acα(2-6)Gal β MP glycoside concentrations with five replicate determinations. The relative standard deviations (RSDs) were 1.48%, 2.30% and 1.11% at the Neu5Acα(2-6)Gal β MP glycoside concentrations of 1 pg mL^{-1}, 1 ng mL^{-1} and 250 ng mL^{-1}, respectively, which demonstrates acceptable precision and good reproducibility.

3.7. Recovery testing

To examine the feasibility of the present electrochemical biosensor for use with authentic samples, the biosensor was applied to human diluted serum samples spiked with 1 pg mL^{-1}, 1 ng mL^{-1} and 100 ng mL^{-1} Neu5Acα(2-6) Gal β MP glycoside, and the recoveries of the three concentrations were 100.8%, 101.2% and 101.4%, and RSDs of the three concentrations were 4.11%, 4.92% and 2.89%, respectively, suggesting acceptable precision.

4. Conclusions

In this study, we fabricated a simple and ultrasensitive electrochemical biosensor based on reduced graphene oxide-

tetraethylene pentamine-$BMIMPF_6$ hybrids for the detection of α2,6-sialylated glycans in human serum. The developed sensor has a broad linear range with a low detection limit and high specificity, suggesting resilience to endogenous interferences in human serum. The biosensor also demonstrates high sensitivity and good reproducibility, making it a potentially advantageous tool for clinical research. However, the fabrication of the biosensor requires multiple steps, which may limit its use and may also have an effect on its stability. Therefore, it is necessary to improve stability further to enhance its use in the detection of α2,6-sialylated glycans in serum and for its application in detecting other proteins or glycans, which will require the use of other affinity binding pairs, such as alternative biosensors, immunosensors and catalysts.

Acknowledgments

This study was supported financially by the National Natural Science Foundation of China (81370403, 21205146).

Appendix A. Supplementary material

Supplementary data associated with this article can be found in the online version at http://dx.doi.org/10.1016/j.bios.2015.07.073.

References

Browna, Billyde, Woltera, Scott D., Stonerb, Brian R., Glass, J.T., 2008. J. Electrochem. Soc. 155 (8), B852–B859.
Boltje, T.J., Buskas, T., Boons, G.J., 2009. Nat. Chem. 1 (8), 611–622.
Bratosin, D., Palii, C., Moicean, A.D., Zanetta, J.P., Montreuil, J., 2007. Biochimie 89 (3), 355–359.
Buzzeo, M.C., Evans, R.G., Compton, R.G., 2004. Chemphyschem 5 (8), 1106–1120.
Cao, X., Wang, N., Jia, S., Guo, L., Li, K., 2013. Biosens. Bioelectron. 39 (1), 226–230.
Claussen, J.C., Franklin, A.D., Ul Haque, A., Porterfield, D.M., Fisher, T.S., 2009. ACS Nano 3 (1), 37–44.
Dall'Olio, F., Malagolini, N., di Stefano, G., Minni, F., Marrano, D., Serafini-Cessi, F., 1989. Int. J. Cancer 44 (3), 434–439.
Fei, X., Zhao, F.Q., Zhang, Y.F., Guo, G.P., Zeng, B.Z., 2009. J. Phys. Chem. C 113 (3), 849–855.
Gao, L., He, J., Xu, W., Zhang, J., Hui, J., Guo, Y., Li, W., Yu, C., 2014. Biosens. Bioelectron. 62, 79–83.
Gessner, P., Riedl, S., Quentmaier, A., Kemmner, W., 1993. Cancer Lett. 75 (3), 143–149.
Guo, A., Li, Y., Cao, W., Meng, X., Wu, D., Wei, Q., Du, B., 2015. Biosens. Bioelectron. 63, 39–46.
Harduin-Lepers, A., Vallejo-Ruiz, V., Krzewinski-Recchi, M.A., Samyn-Petit, B., Julien, S., Delannoy, P., 2001. Biochimie 83 (8), 727–737.
Harvey, D.J., 2011. J. Chromatogr. B Anal. Technol. Biomed. Life Sci. 879 (17–18), 1196–1225.
Jia, H., Gao, P., Ma, H., Wu, D., Du, B., Wei, Q., 2014. Bioelectrochemistry 101C, 22–27.
Jones, C., 2005. J. Pharm. Biomed. Anal. 38 (5), 840–850.
Kim, J.S., Laskowich, E.R., Michon, F., Kaiser, R.E., Arumugham, R.G., 2006. Anal. Biochem. 358 (1), 136–142.
Kim, S., Oh, D.B., Kang, H.A., Kwon, O., 2011. Appl. Microbiol. Biotechnol. 91 (1), 1–15.
Lamari, F.N., Kuhn, R., Karamanos, N.K., 2003. J. Chromatogr. B Anal. Technol. Biomed. Life Sci. 793 (1), 15–36.
Liu, T., Li, J.D., Zeng, R., Shao, X.X., Wang, K.Y., Xia, Q.C., 2001. Anal. Chem. 73 (24), 5875–5885.
Muller, C.I., Lambert, C., 2011. Langmuir 27 (8), 5029–5039.
Park, J.J., Yi, J.Y., Jin, Y.B., Lee, Y.J., Lee, J.S., Lee, Y.S., Ko, Y.G., Lee, M., 2012. Biochem. Pharmacol. 83 (7), 849–857.
Petretti, T., Schulze, B., Schlag, P.M., Kemmner, W., 1999. Biochim. Biophys. Acta 1428 (2–3), 209–218.
Safavi, A., Farjami, F., 2011. Biosens. Bioelectron 26 (5), 2547–2552.
Shafiquzzaman Siddiqueea, Kobun Rovinaa, Yusof, Nor Azah, Rodrigues, Kenneth Francis, Suryania, S., 2014. Sens. Bio-Sens. Res. 2, 16–22.
Shibuya, N., Goldstein, I.J., Broekaert, W.F., Nsimba-Lubaki, M., Peeters, B., Peumans, W.J., 1987. Arch. Biochem. Biophys. 254 (1), 1–8.
Stobiecka, M., Hepel, M., 2011. Biosens. Bioelectron. 26 (8), 3524–3530.
Wu, D., Guo, A., Guo, Z., Xie, L., Wei, Q., Du, B., 2014. Biosens. Bioelectron. 54, 634–639.
Wu, D., Guo, Z., Liu, Y., Guo, A., Lou, W., Fan, D., Wei, Q., 2015. Talanta 134, 305–309.
Xie, S., Zhang, J., Yuan, Y., Chai, Y., Yuan, R., 2015. Chem. Commun. 51 (16), 3387–3390.
Yang, J., Deng, S., Lei, J., Ju, H., Gunasekaran, S., 2011. Biosens. Bioelectron. 29 (1), 159–166.
Yang, J., Zhang, W.D., Gunasekaran, S., 2010. Biosens. Bioelectron. 26 (1), 279–284.
Yuan, G., Yu, C., Xia, C., Gao, L., Xu, W., Li, W., He, J., 2015. Biosens. Bioelectron. 72, 237–246.
Zanetta, Jean-Pierre, Pons, Alexandre, Iwersen, Matthias, Mariller, Christophe, Leroy, Yves, Timmerman, P., Schauer, R., 2001. Glycobiology 11, 663–676.
Zan, X., Fang, Z., Wu, J., Xiao, F., Huo, F., Duan, H., 2013. Biosens. Bioelectron. 49, 71–78.
Zhang, J., He, J., Xu, W., Gao, L., Guo, Y., Li, W., Yu, C., 2015. Electrochim. Acta 156, 45–52.
Zhang, X., Li, F., Wei, Q., Du, B., Wu, D., Li, H., 2014. Sens. Actuators B 194, 64–70.
Zheng, J., Zhang, Y., Yang, P., 2007. Talanta 73 (5), 920–925.